

## Coexistence of strong and weak Majorana zero modes in an anisotropic XY spin chain with second-neighbor interactions

Kazuhiro Wada <sup>1</sup>, Takanori Sugimoto <sup>1,2,\*</sup>, and Takami Tohyama <sup>1</sup>

<sup>1</sup>*Department of Applied Physics, Tokyo University of Science, Tokyo 125-8585, Japan*

<sup>2</sup>*Advanced Science Research Center, Japan Atomic Energy Agency, Tokai, Ibaraki 319-1195, Japan*



(Received 23 March 2021; revised 11 July 2021; accepted 27 July 2021; published 12 August 2021)

We theoretically investigate Majorana zero modes emerging in an anisotropic XY spin chain with second-neighbor interactions. The spin chain is mathematically equivalent to the Kitaev chain comprised of spinless fermions if only nearest-neighbor interactions are considered. Recent studies on the Kitaev chain with long-ranged interactions, have presented coexistence of several Majorana zero modes. Investigating the topological phase diagram of the anisotropic XY spin chain with second-neighbor interactions, we find coexistence of several Majorana zero modes similar to the Kitaev chain. However, we confirm that one of the zero modes is restricted into a Hilbert subspace. The mode is regarded as a so-called weak zero mode that should exhibit thermodynamical properties different from a (strong) zero mode appearing in the whole Hilbert space. Since the quantum statistics of spin is the same as a hard-core boson, we expect an experimental realization of the weak mode in not only quantum spin materials but also optical lattices for cold atom systems.

DOI: [10.1103/PhysRevB.104.075119](https://doi.org/10.1103/PhysRevB.104.075119)

### I. INTRODUCTION

Majorana zero mode (ZM) is a zero-energy excitation defined as a Majorana fermion, whose antiparticle corresponds to itself [1–3]. In condensed matter physics, the Majorana ZM emerging in topological superconductors [4,5] has attracted much attention, because it not only gives fundamental and valuable information of quantum properties originating from non-Abelian statistics [6], but also has a capability to carry out topologically protected quantum computing [7,8] and Majorana qubits [9–14]. For these purposes, realization and control of the Majorana ZMs are urgent issues in current technologies of nano fabrication from both theoretical and experimental points of view [15–37], and moreover these studies bring numerous discussions on the effects of dimerization, quasiperiodicity, disorder, and interaction [38–94].

As a typical topological superconductor, the Kitaev chain is well investigated [5]. In this model, a pairing potential between spinless fermions on neighboring sites plays a key role in topological superconductivity. An alternative to the Kitaev chain is an anisotropic XY spin chain (AXYSC) with  $S = 1/2$  spins given by the Jordan-Wigner transformation of the Kitaev chain [82–87,89–92,94,95]. These models are mathematically equivalent if they have only nearest-neighbor interactions.

Recent studies on long-ranged interactions in the Kitaev chain [45,64,72,96,97] have reported coexistence of several Majorana ZMs [64,72,96]. The increase of Majorana ZMs is in general important for improving efficiency of quantum computing. From an experimental point of view, long-ranged spin interactions, e.g., superexchange couplings, the Ruderman-Kittel-Kasuya-Yosida interactions [98–100],

and dipole-dipole interactions, are more easily introduced as compared with long-ranged superconducting pair potential of spinless fermions appearing in the Kitaev chain. Therefore, in this paper, we investigate the effects of long-ranged interactions in the spin chain, which differ from the long-ranged interactions in the Kitaev chain.

In addition, in connection with non-Abelian statistics, another type of Majorana ZM has also attracted much attention in recent years [69,82,101–103]. The Majorana ZM, the so-called *weak* Majorana ZM, is restricted into a Hilbert subspace including low-lying eigenstates, while the conventional Majorana ZM called *strong* Majorana ZM emerges in the whole Hilbert space. The weak Majorana ZM, which is basically discussed in non-Abelian parafermion systems, behaves in the same manner with the strong Majorana ZM at low temperature. Since the parafermions satisfy an intermediate commutation relation between fermions and hard-core bosons, clarifying behaviors of Majorana ZMs in a spin chain obeying the hard-core bosonic commutation relation is an important study from the quantum statistical point of view.

In contrast to the Kitaev chain, the effects of long-ranged interactions in the spin chain cannot be easily examined due to many-body interactions originating from the Jordan-Wigner string. To overcome this difficulty, we combine numerical calculation based on a variational matrix-product state (VMPS) method [104] with an analytical calculation in the Ising limit. Note that the concept of the VMPS is based on the density-matrix renormalization group (DMRG) method proposed by White [105,106], and thus, the VMPS is mathematically equivalent to the DMRG. In the numerical algorithm, the VMPS, however, has some differences from the DMRG, e.g., the singular-value decomposition of coefficient rectangular matrix of the wave function instead of diagonalization of the reduced density matrix, and matrix-product operator

\*sugimoto.takanori@rs.tus.ac.jp

(MPO) representation of the Hamiltonian as a more sophisticated form of renormalized operators (see Appendix A for the XYSC model). While the VMPS method gives only a few low-lying eigenstates, the analyses of the Ising limit provides all eigenstates because of classical level for special parameters. Combining both the calculations, we can discuss the overall structure in the full Hilbert space to clarify the Majorana ZM.

In this paper, we start with the correspondence between the Kitaev and Ising chains. The Majorana ZM is derived in the Ising chain, and we discuss its features about boundary conditions. In addition, we analytically show a weak Majorana ZM emerging in the Ising chain with second-neighbor interactions. This weak Majorana ZM originating from an extension of unit cell in the ground states is induced by the second-neighbor interactions. Next, to investigate the effects of quantum fluctuations, we present the VMPS study on low-lying eigenstates in the XYSC with second-neighbor interactions. Based on detailed examinations of degeneracy in the low-lying states, we determine the topological phase diagram. To confirm robustness of the weak Majorana ZM against quantum fluctuations, we numerically clarify energy spectra in several parameter points. In these calculations, we find a nontopological phase, where there is no Majorana ZM but a weak *trivial* ZM associated with an extension of unit cell as well as the doubly degenerate Majumdar-Ghosh ground states [107–109]. Finally, we summarize these results and mention possible experiments to find the weak Majorana ZM.

The contents of this paper are as follows. In Sec. II, we introduce the model Hamiltonians of the XYSC and the Kitaev chain together with the Jordan-Wigner transformation. In Sec. III, the Majorana ZMs in the Ising chain are exactly derived as an example of the XYSC. Two types of Majorana ZMs, i.e., strong and weak Majorana ZMs, are demonstrated in the Ising chain. After explaining the VMPS method, we present a topological phase diagram obtained by the VMPS method in Sec. V. As another VMPS result, we also show degeneracy in ground states in Sec. VI. Sections VII and VIII are used for discussion and summary, respectively.

## II. MODEL

We consider the XYSC with a second-neighbor interaction given by

$$\mathcal{H}_S = \sum_{n=1,2} [\mathcal{H}_n^B + \eta \mathcal{H}_n^E], \quad (1)$$

with

$$\mathcal{H}_n^B = \sum_{j=1}^{N-n} [(J_n + \lambda_n) S_j^x S_{j+n}^x + (J_n - \lambda_n) S_j^y S_{j+n}^y], \quad (2)$$

$$\mathcal{H}_n^E = \sum_{j=1}^n [(J_n + \lambda_n) S_{N-n+j}^x S_j^x + (J_n - \lambda_n) S_{N-n+j}^y S_j^y], \quad (3)$$

where  $\mathcal{H}_n^B$  ( $\mathcal{H}_n^E$ ) is the bulk (edge) Hamiltonian of  $n$ th neighbor interaction for  $n = 1, 2$  (see Appendix A for the MPO representation). The  $x$  ( $y$ ) component of the spin-1/2 operator on the  $j$ th site is denoted by  $S_j^x$  ( $S_j^y$ ). The exchange energy and anisotropy of the  $n$ th neighbor coupling are defined as

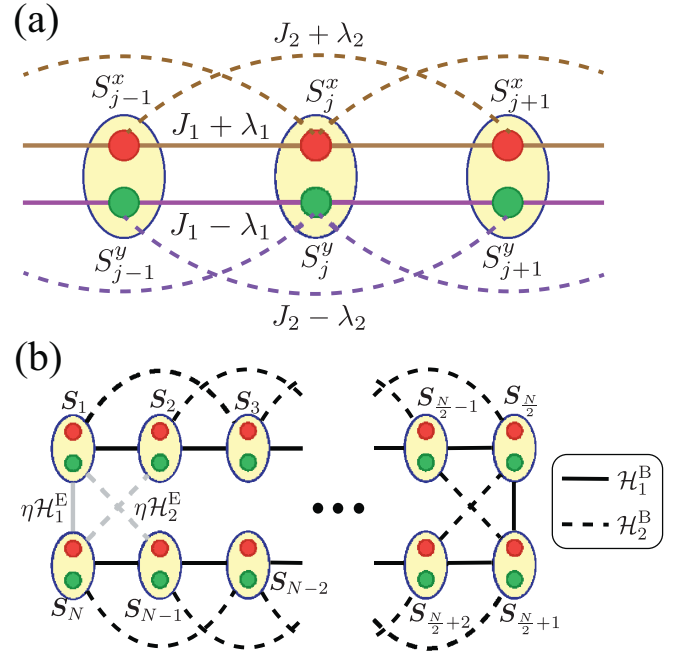


FIG. 1. Schematics of the XYSC. Red (green) balls represent  $x$  ( $y$ ) components of the spin-1/2 operator. The spin operator except for the  $z$  component is denoted by a yellow oval. Solid and dashed lines are the first- and second-neighbor interactions, respectively. (a) The anisotropic interactions of  $x$  ( $y$ ) components are colored brown (purple). (b) The bulk (edge) Hamiltonian is colored black (gray). Without the edge Hamiltonian ( $\eta = 0$ ), the system corresponds to the open boundary condition (OBC), while the periodic boundary condition (PBC) is chosen with  $\eta = 1$ .

$J_n$  and  $\lambda_n$ , respectively (see Fig. 1). To control the boundary condition, we use the parameter  $\eta$ .

The Majorana ZM emerges on the edges in a topological phase of a one-dimensional  $p$ -wave superconductor (the Bogoliubov–de Gennes class) [110], e.g., the Kitaev chain, with the open boundary condition (OBC). The Kitaev chain of the  $n$ th neighbor interaction is given by

$$\mathcal{H}_n^K = \sum_{j=1}^{N-n} (t_n c_j^\dagger c_{j+n} + \Delta_n c_j^\dagger c_{j+n}^\dagger + \text{H. c.}), \quad (4)$$

where  $c_j^\dagger$  ( $c_j$ ) denotes the creation (annihilation) operator of spinless fermion on the  $j$ th site. The Kitaev chain with only the first-neighbor interaction  $\mathcal{H}_1^K$  is mathematically equivalent to the XYSC  $\mathcal{H}_1^B$  with  $2t_1 = J_1$  and  $2\Delta_1 = \lambda_1$  through the Jordan-Wigner transformation [95],

$$S_j^+ = c_j^\dagger \prod_{k=1}^{j-1} e^{-i\pi n_k}, \quad S_j^- = c_j \prod_{k=1}^{j-1} e^{i\pi n_k}, \quad (5)$$

where  $n_j = c_j^\dagger c_j$  represents the number operator of spinless fermion on the  $j$ th site. The topological bulk state in the Kitaev chain has a finite energy gap, so that the Majorana ZM is also expected in the XYSC model with small  $J_2$  and  $\lambda_2$  as compared with  $J_1$  and  $\lambda_1$  under OBC ( $\eta = 0$ ). Furthermore, preceding works have pointed out that a second-neighbor interaction  $\mathcal{H}_2^K$  in the Kitaev model induces multiple Majorana

ZMs [64,72,96]. However, the second-neighbor interaction  $\mathcal{H}_2^B$  in the AXYS model discords with  $\mathcal{H}_2^K$  in the Kitaev model, because the Jordan-Wigner phase of a middle site, the so-called Jordan-Wigner string, does not cancel out after the transformation, that is,

$$\mathcal{H}_2^B = \frac{1}{2} \sum_{j=1}^{N-2} (J_2 c_j^\dagger e^{i\pi n_{j+1}} c_{j+2} + \lambda_2 c_j^\dagger e^{i\pi n_{j+1}} c_{j+2}^\dagger + \text{H. c.}). \quad (6)$$

Thus, it is an interesting problem to clarify whether  $\mathcal{H}_2^B$  in the AXYS model also induces multiple Majorana ZMs as well as  $\mathcal{H}_2^K$  in the Kitaev chain.

### III. MAJORANA ZMS IN ISING CHAIN

We first demonstrate the Majorana ZM appearing in the Ising chain as the classical limit of the AXYS. The Majorana ZM is a zero-energy quasiparticle excitation which obeys the Majorana condition, i.e., its Hermitian conjugate is the same as itself. Two types of Majorana operators  $\gamma_j^\tau$  ( $\tau = a, b$ ) satisfying the Majorana condition  $\gamma_j^\tau = (\gamma_j^\tau)^\dagger$  are introduced by one fermion:

$$\gamma_j^a = \frac{1}{\sqrt{2}}(c_j^\dagger + c_j), \quad \gamma_j^b = \frac{i}{\sqrt{2}}(c_j^\dagger - c_j). \quad (7)$$

These operators obey the fermionic anticommutation relation  $\{\gamma_j^\tau, \gamma_{j'}^{\tau'}\} = \delta_{j,j'} \delta_{\tau,\tau'}$ . Moreover, the Majorana operator can be regarded as an operator which changes the fermion-number parity given by

$$\mathcal{F} = e^{i\pi \sum_j n_j} = \prod_j 2i\gamma_j^b \gamma_j^a. \quad (8)$$

In fact, the Majorana operators anticommute with the fermionic parity  $\{\gamma_j^\tau, \mathcal{F}\} = 0$ , and the fermionic parity is conserved in the AXYS,  $[\mathcal{F}, \mathcal{H}_S] = 0$ . Thus, with considering a simultaneous eigenstate of the Hamiltonian and the fermionic parity  $|\varepsilon, \chi\rangle$  with eigenenergy  $\varepsilon$  and the eigenvalue of the fermionic parity  $\chi = \pm 1$ , the state obtained by the Majorana operator acting on an eigenstate has an opposite parity to the eigenstate:

$$\mathcal{F}(\gamma_j^\tau |\varepsilon, \chi\rangle) = -\chi(\gamma_j^\tau |\varepsilon, \chi\rangle). \quad (9)$$

Furthermore, if there is a Majorana operator  $\tilde{\gamma}$  commuting with the Hamiltonian  $[\tilde{\gamma}, \mathcal{H}_S] = 0$ , a pair of eigenstates with different fermionic parity exists at every energy level,  $|\varepsilon, \chi\rangle$  and  $|\varepsilon, -\chi\rangle \equiv \sqrt{2}\tilde{\gamma} |\varepsilon, \chi\rangle$ . This Majorana operator  $\tilde{\gamma}$  is called (strong) Majorana ZM. Besides the commutation relation  $[\tilde{\gamma}, \mathcal{H}_S] = 0$ , recent theoretical study has predicted the Majorana ZM satisfying a weaker condition  $\mathcal{P}[\tilde{\gamma}_\bullet, \mathcal{H}_S]\mathcal{P} = 0$  with a projection to a certain Hilbert subspace  $\mathcal{P}$  [69,82,101–103]. In this case, only eigenstates belonging to the subspace are doubly degenerate. The Majorana ZM  $\tilde{\gamma}_\bullet$  with such a weaker condition  $\mathcal{P}[\tilde{\gamma}_\bullet, \mathcal{H}_S]\mathcal{P} = 0$  is called *weak* Majorana ZM, as compared with the strong Majorana ZM  $\tilde{\gamma}$  satisfying  $[\tilde{\gamma}, \mathcal{H}_S] = 0$ .

We can easily find the strong Majorana ZM in the Ising chain without the second-neighbor interaction, corresponding to a condition  $\lambda_1 = \pm J_1$  in the AXYS. For instance, the

Majorana representation of the Ising chain is given by

$$\mathcal{H}_1^B|_{\lambda_1=J_1} = -J_1 \sum_{j=1}^{N-1} i\gamma_j^b \gamma_{j+1}^a. \quad (10)$$

Two Majorana operators  $\gamma_1^a$  and  $\gamma_N^b$  on the edges apparently commute with the Hamiltonian, indicating two strong Majorana ZMs  $\tilde{\gamma}^a = \gamma_1^a$  and  $\tilde{\gamma}^b = \gamma_N^b$  existing in the Ising chain. These Majorana ZMs  $\tilde{\gamma}^a$  and  $\tilde{\gamma}^b$  are essentially the same Majorana ZM. The reason is as follows. The Hermite operator  $2i\tilde{\gamma}^a \tilde{\gamma}^b$ , which has two eigenvalues  $\chi_e = \pm 1$ , commutes with both the Hamiltonian  $\mathcal{H}_1^B|_{\lambda_1=J_1}$  and the fermionic parity  $\mathcal{F}$ , so that there are simultaneous eigenstates  $|\varepsilon, \chi, \chi_e\rangle$ . With applying  $\tilde{\gamma}^a$  on the eigenequation of  $2i\tilde{\gamma}^a \tilde{\gamma}^b$ , we obtain the following relation:

$$\tilde{\gamma}^b |\varepsilon, \chi, \chi_e\rangle = -i\chi_e \tilde{\gamma}^a |\varepsilon, \chi, \chi_e\rangle. \quad (11)$$

These two states are the same without the phase factor  $-i\chi_e$ , and thus, the Majorana ZMs  $\tilde{\gamma}^a$  and  $\tilde{\gamma}^b$  are essentially equivalent (see Appendix B for more information of these Majorana ZMs). Interestingly, these strong Majorana ZMs survive with periodic boundary condition (PBC) in the Ising chain, that is, the  $\tilde{\gamma}^a$  and  $\tilde{\gamma}^b$  also commute with the edge Hamiltonian,

$$\mathcal{H}_1^E|_{\lambda_1=J_1} = -iJ_1 \gamma_N^b \gamma_1^a \mathcal{F}. \quad (12)$$

This startling feature originates from the operator  $\mathcal{F}$  as a remnant of the Jordan-Wigner transformation, and thus, this feature is inherent in the spin chain. In a general case with  $J_1 \neq \lambda_1$ , a strong Majorana ZM is obtained as a superposition of Majorana operators. In the Kitaev chain with OBC, this mode is slightly expanded from edges but exponentially decreasing into the bulk. Thus, it is exactly obtained only in the thermodynamic limit.

Next, let us consider the effects of the second-neighbor interaction in the Ising chain with PBC ( $\lambda_1 = J_1$  and  $\lambda_2 = J_2$ ). In the following, the system size  $N$  is set to satisfy  $N = 0 \pmod{4}$ , and the interactions are restricted into antiferromagnetic  $J_1 > 0$  and  $J_2 > 0$  for simplicity. The ground-state phase undergoes the first-order phase transition at  $J_1^x = 2J_2^x$ , where the degeneracy of ground states changes from twofold ( $J_1^x > 2J_2^x$ ) to fourfold ( $J_1^x < 2J_2^x$ ). In the latter region  $J_1^x < 2J_2^x$ , the fourfold ground states are given by

$$|gs_1\rangle = |\uparrow\uparrow\downarrow\downarrow\cdots\rangle_x, \quad |gs_2\rangle = |\downarrow\downarrow\uparrow\uparrow\cdots\rangle_x, \quad (13)$$

$$|gs_3\rangle = |\uparrow\downarrow\downarrow\uparrow\cdots\rangle_x, \quad |gs_4\rangle = |\downarrow\uparrow\uparrow\downarrow\cdots\rangle_x, \quad (14)$$

where  $|\uparrow\downarrow\downarrow\uparrow\cdots\rangle_x$  is defined as a direct product,  $|\uparrow\rangle_1^x |\downarrow\rangle_2^x |\uparrow\rangle_3^x |\downarrow\rangle_4^x \cdots$  with the eigenstates of  $S_j^x$ ,  $|\uparrow\rangle_j^x$ , and  $|\downarrow\rangle_j^x$ . To diagonalize the fermionic parity in these states, we adopt bonding and antibonding ground states as linear combinations of these states:

$$|gs_{1,2}^\pm\rangle = \frac{1}{\sqrt{2}}(|gs_1\rangle \pm |gs_2\rangle),$$

$$|gs_{3,4}^\pm\rangle = \frac{1}{\sqrt{2}}(|gs_3\rangle \pm |gs_4\rangle). \quad (15)$$

With the relations  $|\downarrow\rangle_j^x = -e^{i\pi n_j} |\uparrow\rangle_j^x$  and  $|\uparrow\rangle_j^x = -e^{i\pi n_j} |\downarrow\rangle_j^x$ , where  $e^{i\pi n_j}$  corresponds to a spin-flip operator of the

$x$  component, eigenequations of the fermionic parity are obtained by

$$\mathcal{F} |\text{gs}_{1,2}^{\pm}\rangle = \pm |\text{gs}_{1,2}^{\pm}\rangle, \quad \mathcal{F} |\text{gs}_{3,4}^{\pm}\rangle = \pm |\text{gs}_{3,4}^{\pm}\rangle. \quad (16)$$

Thus, there is a Majorana ZM between the bonding and antibonding ground states. This characteristic is common to all energy levels. In fact, every state can be written by a direct product of local eigenstate  $|\uparrow\rangle_j^x$  or  $|\downarrow\rangle_j^x$ , e.g.,  $|\psi\rangle = |\uparrow\uparrow\downarrow\uparrow\cdots\rangle_x$ . The direct product state  $|\psi\rangle$  has a spin-flip pair  $\mathcal{F}|\psi\rangle = |\downarrow\downarrow\uparrow\downarrow\cdots\rangle_x$ , which has the same energy as  $|\psi\rangle$ . The bonding and antibonding states  $|\psi_{\pm}\rangle = (|\psi\rangle \pm \mathcal{F}|\psi\rangle)/\sqrt{2}$  have different fermionic parity. Therefore, this Majorana ZM between bonding and antibonding states at each energy level corresponds to a strong Majorana ZM,  $\tilde{\gamma}^a = \sum_{\psi} (|\psi_+\rangle \langle\psi_-| + |\psi_-\rangle \langle\psi_+|)/\sqrt{2}$ , e.g.,  $\tilde{\gamma}^a = \sqrt{2}S_1^x$ .

On the other hand, there is another Majorana ZM in the ground states, i.e., a Majorana ZM between  $|\text{gs}_{1,2}^+\rangle$  and  $|\text{gs}_{3,4}^-\rangle$  ( $|\text{gs}_{1,2}^-\rangle$  and  $|\text{gs}_{3,4}^+\rangle$ ). This mode is constructed by the spin-flip operator of odd sites  $\mathcal{F}_o$  and the parity-flip operator  $S_1^x$ , i.e.,  $\tilde{\gamma}_o^a = \sqrt{2}iS_1^x\mathcal{F}_o$ . This operator also satisfies the Majorana condition  $\{\tilde{\gamma}_o^a, \tilde{\gamma}_o^a\} = 0$ ,  $2(\tilde{\gamma}_o^a)^2 = 1$ , and  $\tilde{\gamma}_o^a = (\tilde{\gamma}_o^a)^{\dagger}$ . However, for instance, with respect to the highest-energy (saturated) states  $|\uparrow\uparrow\uparrow\cdots\rangle_x$  and  $|\downarrow\downarrow\downarrow\cdots\rangle_x$ , which are only doubly degenerate,  $\tilde{\gamma}_o^a$  corresponds to a Majorana mode in a different energy sector. The difference of degeneracy originates from  $\mathcal{P}[\tilde{\gamma}_o^a, \mathcal{H}_S]\mathcal{P} = 0$  with a projection  $\mathcal{P}$  to a certain Hilbert subspace including the ground states but except for the saturated states. Therefore, this mode is regarded as a weak Majorana ZM.

It is also worth noting that this weak Majorana ZM is regarded as a product of the strong Majorana ZM  $\tilde{\gamma}^a$ , the fermionic parity  $\mathcal{F}$ , and a weak (not Majorana) ZM, that we call a weak *trivial* ZM in this paper, between  $|\text{gs}_{1,2}^+\rangle$  and  $|\text{gs}_{3,4}^+\rangle$  ( $|\text{gs}_{1,2}^-\rangle$  and  $|\text{gs}_{3,4}^-\rangle$ ). This weak trivial ZM corresponds to a translation operator  $\mathcal{T}$  defined by

$$|\text{gs}_1\rangle = \mathcal{T} |\text{gs}_3\rangle, \quad |\text{gs}_2\rangle = \mathcal{T} |\text{gs}_4\rangle. \quad (17)$$

In the ground states, the translation operator  $\mathcal{T}$  is equivalent to the spin-flip operator of even sites  $\mathcal{F}_e$ , i.e.,  $\mathcal{P}\mathcal{T}\mathcal{P} = \mathcal{P}\mathcal{F}_e\mathcal{P}$ . Thus, we can obtain the relation  $\tilde{\gamma}_o^a = i\tilde{\gamma}^a\mathcal{F}\mathcal{T}$  in the ground states.

More generally, if there is a trivial ZM  $\zeta$  defined by any parity-flip operator ( $\zeta^2 = 1$ ), commuting with another (intrinsic) Majorana ZM  $\tilde{\gamma}$ , the fermionic parity  $\mathcal{F}$ , and the Hamiltonian  $\mathcal{H}$ , i.e.,  $[\zeta, \tilde{\gamma}] = [\zeta, \mathcal{F}] = [\zeta, \mathcal{H}] = 0$ , a product of them,  $\tilde{\gamma}' = i\tilde{\gamma}\mathcal{F}\zeta$ , satisfies the Majorana ZM conditions independent from the  $\tilde{\gamma}$ , namely,  $\{\tilde{\gamma}', \tilde{\gamma}'\} = \{\tilde{\gamma}', \mathcal{F}\} = [\tilde{\gamma}', \mathcal{H}] = 0$ ,  $2(\tilde{\gamma}')^2 = 1$ , and  $\tilde{\gamma}' = (\tilde{\gamma}')^{\dagger}$ . To avoid misunderstanding, we again insist that this Majorana ZM  $\tilde{\gamma}'$  is different from the pair to the Majorana ZM  $\tilde{\gamma}$  (see Appendix C for more information). Moreover, it is intriguing that this reconstructed Majorana ZM  $\tilde{\gamma}'$  can exist only with the intrinsic Majorana ZM  $\tilde{\gamma}$ , otherwise there is just a trivial ZM. In the Ising chain with large enough second-neighbor interactions, unit cell of the ground state is extended twice as large as the Néel state, resulting in generation of sublattice degree of freedom associated with the translation. This degree of freedom corresponds to the weak trivial ZM ( $\zeta$ ) in the ground states, so that we

can find a weak Majorana ZM ( $\tilde{\gamma}'$ ) if there is another strong Majorana ZM ( $\tilde{\gamma}$ ).

#### IV. NUMERICAL METHOD

In general, the Majorana ZM in the AXYSK with second-neighbor interactions is not easy to be clarified due to quantum fluctuation. To clarify the quantum effects, we investigate low-lying states with the VMPS method. In this study, we set the bond dimension of the VMPS to be greater than 400 and confirmed that truncation error is approximately less than  $10^{-6}$ . If there is a degeneracy in the ground states with different fermionic parities, we can confirm at least existence of a weak Majorana ZM. Moreover, we can discuss the type of ZMs by comparison with the Ising chain. The number and type of Majorana ZMs can help us to determine the ground-state phase diagram.

In the AXYSK, the strong Majorana ZM is not localized in the edges, and thus, we can detect the Majorana ZM with both OBC and PBC by checking the degeneracy of the ground states. In addition, the bulk state is common between OBC and PBC in the thermodynamical limit, so that the topological phase diagrams with OBC and PBC should be the same. Thus, to determine the topological phase diagram, we choose the OBC to reduce the numerical costs of the VMPS method. On the other hand, as explained in Sec. III, the translational symmetry is crucial in finding the weak trivial ZM, irrespective of existence of the strong Majorana ZM. Since the OBC breaks the translational symmetry, we apply the PBC when we discuss the existence of the weak trivial ZM. Note that even with the OBC, we can find the phase transition related to the weak trivial ZM of the PBC, because the first-excitation gap closes at the transition point. If there is the strong Majorana ZM, the weak trivial ZM is regarded as an additional Majorana ZM (see Appendix C). Therefore, we can obtain a more detailed classification of the topological phase diagram in light of the weak trivial ZM.

To obtain the ground-state energy in specified parity subspaces, we add an auxiliary field in the Hamiltonian defined by

$$\mathcal{H}_F = \mu \sum_{\alpha} |\mathcal{F}^{\alpha} - \chi^{\alpha}\rangle, \quad (18)$$

where  $\mathcal{F}^{\alpha} = \prod_{j=1}^N (-2S_j^{\alpha})$  is the  $\alpha = x, y, z$  component of the parity operator, which is conserved in the Hamiltonian because of  $[\mathcal{F}^{\alpha}, \mathcal{H}_S] = 0$ . The fermionic parity  $\mathcal{F}$  in Sec. III corresponds to the  $z$  component  $\mathcal{F}^z$ . These parity operators have  $Z_2$  quantities according to their eigenvalues, while there is a constraint  $\mathcal{F}^x\mathcal{F}^y\mathcal{F}^z = (-i)^N$ . For simplicity, in this paper, we consider only the  $N = 4n$  system size with a positive integer  $n$ , so that acceptable subspaces distinguished by eigenvalues of the parities,  $\chi_i = (\chi_i^x, \chi_i^y, \chi_i^z)$ , are given by

$$\begin{aligned} \chi_0 &= (+, +, +), & \chi_1 &= (+, -, -), \\ \chi_2 &= (-, +, -), & \chi_3 &= (-, -, +), \end{aligned} \quad (19)$$

where  $\chi_i^{\alpha}$  denotes each eigenvalue of the parity operator  $\mathcal{F}^{\alpha}$  [111]. Therefore, with a fixed  $\chi$  for the target subspace, we can calculate the ground-state energy using the VMPS

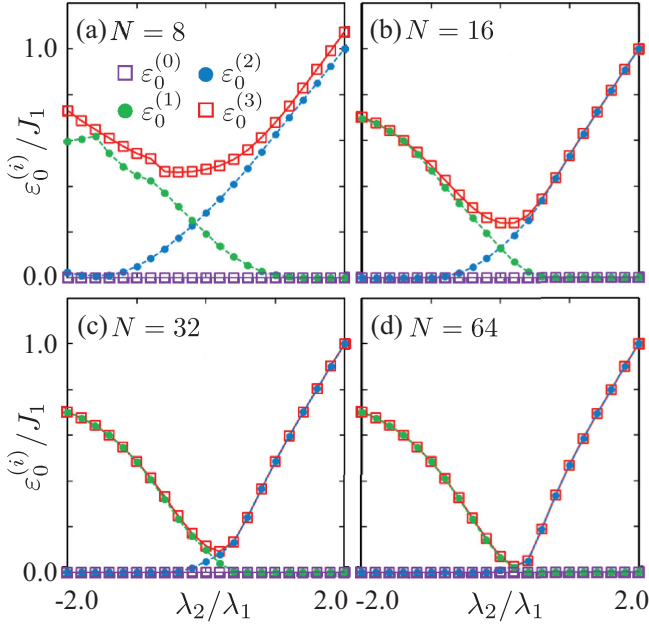


FIG. 2. Size dependence of ground-state energies  $\varepsilon_0^{(i)}$  in four subspaces with different parity  $\chi_i$  for  $i = 0, 1, 2, 3$ , corresponding to  $(+, +, +)$ ,  $(+, -, -)$ ,  $(-, +, -)$ ,  $(-, -, +)$  with fixed  $\lambda_1/J_1 = 1$  ( $\theta = \pi/4$ ) and  $J_2/J_1 = 2$  for (a)  $N = 8$ , (b)  $N = 16$ , (c)  $N = 32$ , and (d)  $N = 64$  systems. The real ground-state energy  $\varepsilon_0^{(0)}$  is set to be zero.

method for  $\mathcal{H}_S + \mathcal{H}_F$  with a large enough positive potential  $\mu > 0$  (see Appendix A for the MPO representation).

Furthermore, to clarify the degeneracy in the same subspace, we also calculate the  $\nu$ th lowest eigenenergy  $\varepsilon_\nu$  after obtaining up to  $(\nu - 1)$ th low-lying eigenstates  $|l\rangle$  ( $l = 0, 1, 2, \dots, \nu - 1$ ). In the VMPS method, we can obtain any excitation energy with shifting all low-lying states to upper levels. To shift the low-lying states, we introduce an additional term defined by

$$\mathcal{H}_L = \varepsilon \sum_{l=0}^{\nu-1} |l\rangle \langle l|. \quad (20)$$

With applying an energy shift larger than  $\nu$ th excitation energy,  $\varepsilon > \varepsilon_\nu - \varepsilon_0$ , the lowest-energy state corresponds to the  $\nu$ th eigenstate, since the Hamiltonian is deformed into  $\mathcal{H}_S + \mathcal{H}_L = \sum_{l \geq \nu} \varepsilon_l |l\rangle \langle l| + \sum_{l < \nu} (\varepsilon_l + \varepsilon) |l\rangle \langle l|$ . Thus, if we separately set the shift energy to the eigenenergy, i.e.,  $\varepsilon = -\varepsilon_l$ , the effect of  $\mathcal{H}_L$  corresponds to the projection into the Hilbert subspace perpendicular to the subspace comprised of the low-lying eigenvectors  $|l\rangle$  ( $l = 0, 1, \dots, \nu - 1$ ).

## V. TOPOLOGICAL PHASE DIAGRAM

In this section, we present the topological phase diagram of the AXYS, which is determined by the degeneracy and parities of ground states with OBC. The degeneracy and parities are clarified by the VMPS method with the auxiliary field (see Sec. IV). Since the Majorana ZMs in the AXYS emerge in the thermodynamic limit, we first confirm the size effects.

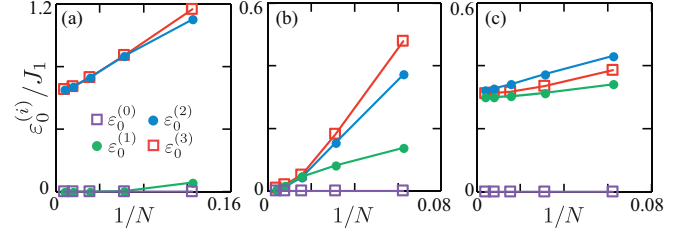


FIG. 3. Size dependence of ground-state energies  $\varepsilon_0^{(i)}$  in four subspaces  $\chi_i$ . The parameter points are  $(\theta, J_2/J_1, \lambda_2/\lambda_1) =$  (a)  $(\pi/4, 2.0, 0.8)$ , (b)  $(\pi/4, 2.0, 0.2)$ , and (c)  $(7\pi/20, 1.2, 0.2)$ .

Figure 2 shows the size dependence of the ground-state energies in four subspaces  $\chi_i$  ( $i = 0, 1, 2, 3$ ), which are identified by the three-component parities  $\mathcal{F}^\alpha$ . With increasing the system size  $N$ , i.e., from (a) to (d), the energies converge into two levels with twofold degeneracy. In (d), the ground states in  $\chi_0$  and  $\chi_2$  ( $\chi_1$  and  $\chi_3$ ) are degenerate for  $\lambda_2/\lambda_1 \lesssim 0.2$ , while the ground states in  $\chi_0$  and  $\chi_1$  ( $\chi_2$  and  $\chi_3$ ) are degenerate for  $\lambda_2/\lambda_1 \gtrsim 0.2$ .

Next, to clarify the size dependence in more detail, we show the ground-state energies as a function of inverse system size  $1/N$ , in which we can apparently check the thermodynamical limit. In Fig. 3, the size dependence of ground-state energies in subspaces is shown at certain parameter points,  $(\theta, J_2/J_1, \lambda_2/\lambda_1) = (\pi/4, 2.0, 0.8)$ ,  $(\pi/4, 2.0, 0.2)$ , and  $(7\pi/20, 1.2, 0.2)$ . In Fig. 3(a), we can see the convergence of energies into two energy levels corresponding to the strong Majorana ZM. On the other hand, we can see the convergence of energies into one energy level in Fig. 3(b) (see also Fig. 2), indicating the phase boundary. Moreover, we can find parameter points where no degeneracy exists at the ground state like Fig. 3(c), implying no Majorana ZMs. Based on these behaviors, we have classified the topological phase diagram.

Since the parity component associated with degeneracy changes at the topological phase boundary, the fourfold degeneracy in the ground state helps us draw a topological ground-state phase diagram. In Fig. 4, we show the phase diagram, where there are three parameters  $\lambda_1/J_1$  represented by  $\theta = \tan^{-1}(\lambda_1/J_1)$ ,  $J_2/J_1$ , and  $\lambda_2/\lambda_1$ . We find three phases distinguished by the degeneracy and the parity components: two topological phases with different parities [(light and dark) green, and blue regions] and a nontopological phase without degeneracy between different parities (orange region). In the (light and dark) green regions, the ground states are degenerate between  $\chi_0$  and  $\chi_1$  subspaces, while in the blue region, the ground-state degeneracy exists between  $\chi_0$  and  $\chi_2$  subspaces. On the other hand, we do not find the ground-state degeneracy between different parity subspaces in the orange region, indicating that two-body interactions in second-neighbor terms break topological ground state and Majorana ZMs.

Next, we explain the equivalence of the separated blue regions and the difference of the two green regions. On  $\theta = \pi/4$ , corresponding to  $J_1 = \lambda_1$ , there is a mirror symmetry with respect to the diagonal line (Ising limit), because the Hamiltonian  $\mathcal{H}_2^B$  is invariant under permutation of  $J_2$  and  $\lambda_2$  with a distinct spin rotation around the  $x$  axis  $S_j^y \rightarrow -S_j^y$  for  $j = 0, 1 \pmod{4}$ . Note that the spin

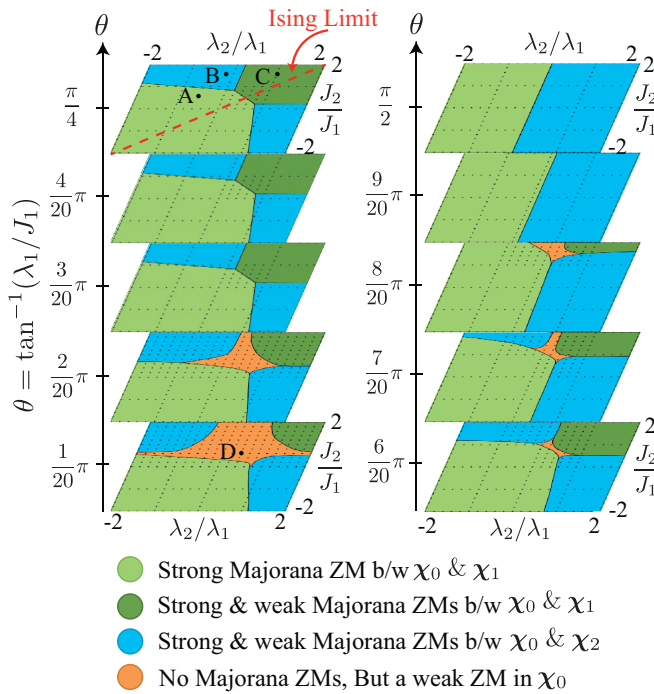


FIG. 4. Topological phase diagram of the XYSC with second-neighbor interaction. In the light- and dark-green regions, the ground state exhibits the Majorana ZM between  $\chi_0$  and  $\chi_1$  subspaces, whereas in the blue region, the Majorana ZM exists between  $\chi_0$  and  $\chi_2$  subspaces. Except for a common fermionic parity  $\mathcal{F}^z$ , the green and blue topological phases are characterized by the fermionic parities  $\mathcal{F}^y$  and  $\mathcal{F}^x$ , respectively. In the orange region, there is no degeneracy between different parity subspaces. The calculation is performed for an  $N = 64$  system with OBC. The parameter points A ( $\theta = \pi/4, J_2/J_1 = 0.6, \lambda_2/\lambda_1 = -0.6$ ), B ( $\theta = \pi/4, J_2/J_1 = 1.6, \lambda_2/\lambda_1 = -0.2$ ), C ( $\theta = \pi/4, J_2/J_1 = 1.6, \lambda_2/\lambda_1 = 1.0$ ), and D ( $\theta = \pi/20, J_2/J_1 = 0.6, \lambda_2/\lambda_1 = 0.4$ ) are used to demonstrate correlation functions (see Fig. 5) and degeneracy at the ground states (see Sec. VI). The red dashed line denotes the Ising chain with second-neighbor interactions, where  $J_2/J_1 = \lambda_2/\lambda_1$  at  $\theta = \pi/4$  ( $\lambda_1/J_1 = 1$ ).

rotation also keeps the parity operators  $\mathcal{F}^\alpha$ . Accordingly, the left-upper topological phase (a blue region) is identical to the right-lower topological phase (the other blue region) at least on  $\theta = \pi/4$ . Since every blue region on each  $\theta$  panel should be continuously connected to each other, we conclude that blue regions are the same phase.

However, recalling the phase transition in the Ising chain with the PBC, the light- and dark-green regions are not regarded as the same phase. As explained in Sec. III, the ground state in the Ising chain comes across the phase transition at  $J_1^x = 2J_2^x$ , corresponding to the crossing point of the black line and the red dashed line on  $\theta = \pi/4$  in Fig. 4, where degeneracy of the ground states changes from twofold to fourfold with increasing  $J_2 = \lambda_2$ . In fact, we find that there is a sign of topological transition on the phase boundary between light- and dark-green regions, where all ground states in different four-parity subspaces are degenerate (not shown) as for the phase boundaries between the blue and green regions.

To confirm the phase transition accompanying the doubly extended unit cell with spontaneous breaking of translational

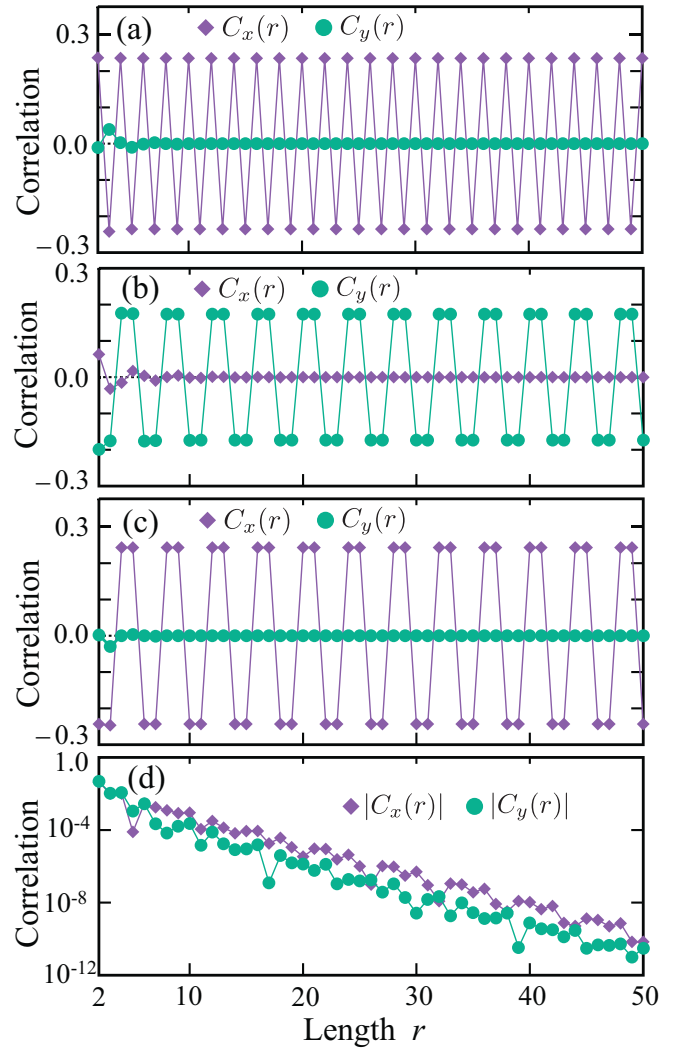


FIG. 5. Correlation functions  $C_\alpha(r)$  for  $\alpha = x, y$  in the ground state at the four parameter points A, B, C, and D in Fig. 4. We calculate the ground state without any auxiliary fields  $\mathcal{H}_F$  and  $\mathcal{H}_L$ , i.e.,  $\mu = \epsilon = 0$ , in an  $N = 256$  system with OBC.

symmetry, we show the correlation functions of  $\alpha = x, y$  components of spins defined by

$$C_\alpha(r) = \langle S_{N/2}^\alpha S_{N/2+r}^\alpha \rangle. \quad (21)$$

The correlation functions at the four parameter points A, B, C, and D in Fig. 4, representing the light-green, blue, dark-green, and orange regions, respectively. By comparison between A and C in Fig. 5, we can see that the periods of  $C_x(r)$  are different. In addition, we can also confirm that the  $y$  component of the spin correlations  $C_y(r)$  shows a long-range order in B, while in A and C, the  $x$  component  $C_x(r)$  is long ranged. On the other hand, in D, there is no long-range order of spins, because both the correlation functions  $|C_\alpha(r)|$  exponentially decrease with increasing the length  $r$ .

Although the weak Majorana ZM is also expected off the diagonal line (Ising limit) in the dark-green region, it is difficult to prove it analytically. In the next section, we demonstrate the ground-state degeneracy at four points A, B,

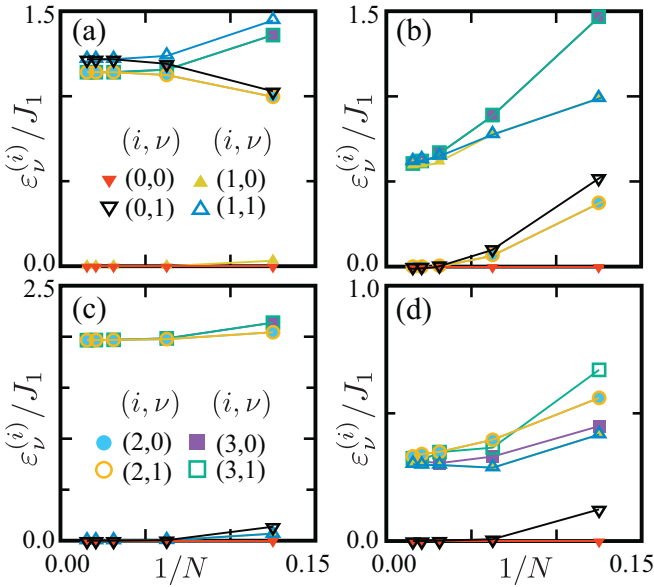


FIG. 6. Size dependence of the ground-state ( $\nu = 0$ ) and first-excitation ( $\nu = 1$ ) energies in four subspaces  $\chi_i$  ( $i = 0, 1, 2, 3$ ), by means of the VMPS method in the  $N = 8, 16, 32, 48, 64$  AXYSs with the PBC. Four panels correspond to the points A, B, C, and D in Fig. 4. In each panel, closed (open) symbols denote the ground-state (first-excitation) energies with four different shapes, upward triangle, downward triangle, circle, and square corresponding to the subspace indices  $i = 0, 1, 2$ , and  $3$ , respectively. The energy origin is set to the minimal energy of the ground-state energies.

C, and D, representing the light-green, blue, dark-green, and orange regions, respectively.

## VI. GROUND-STATE DEGENERACY AND WEAK MAJORANA ZM

To confirm the degeneracy associated with the weak Majorana ZM in topological phases, we numerically obtain lowest energies with PBC at three points A, B, and C at  $\theta = \pi/4$  ( $J_1 = \lambda_1$ ) in Fig. 4 by means of the VMPS method.

Figure 6 shows the size dependence of the ground-state and first-excitation energies in all subspaces, where strong quantum fluctuations exist contrary to the Ising limit. We have confirmed that the numerical overlap between the ground and first-excited states in the same subspace is negligibly small,  $|\langle 0|1\rangle| \lesssim 10^{-5}$ . In all panels, we can see the convergence of energies to approximately two or three levels with increasing the system size.

To check the degeneracy more closely, we present the ground-state and first-excitation energies of the  $N = 64$  AXYS in Fig. 7. In contrast to the point A, we can see fourfold degeneracy in the points B and C, whereas both the points A and C belong to the (light- and dark-) green regions where the ground states are degenerate between the  $\chi_0$  and  $\chi_1$  subspaces. Hence, the degeneracy is unchanged even in the presence of quantum fluctuation.

In the dark-green region, as we explained in Sec. III, there is a weak Majorana ZM in addition to the strong Majorana ZM in the Ising limit, indicating that some excited states are only twofold degenerate. At least in a certain region near the Ising

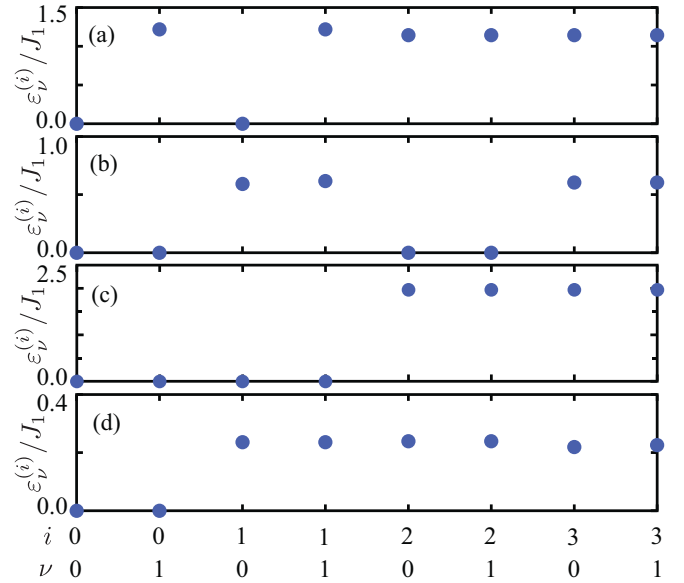


FIG. 7. Ground-state and first-excitation energies obtained by the VMPS method in the  $N = 64$  AXYS with the PBC. Panels from top to bottom correspond to the energy spectra at the points A, B, C, and D in Fig. 4. The horizontal axis represents the index of the subspace ( $i = 0, 1, 2, 3$ ) and state number  $\nu = 0, 1$ ; i.e., ground state ( $\nu = 0$ ) and first excitation ( $\nu = 1$ ) in the  $\chi_i$  subspace.

limit, the excited states are still twofold degenerate, while degeneracy of the ground states should be fourfold even if quantum fluctuations exist. Therefore, we conclude that the weak Majorana ZM survives not only in the classical Ising limit but with quantum fluctuations, although we cannot deny the existence of two strong Majorana ZMs, i.e., a shift of Majorana ZM from weak to strong mode, in a part of the dark-green region.

On the other hand, we find ground-state degeneracy even in the nontopological phase without Majorana ZMs (orange region in Fig. 4). This degeneracy in the same subspace does not exist in the light-green region, which corresponds to the topological phase in the Kitaev chain with only first-neighbor terms. Therefore, this degeneracy is also induced by the second-neighbor interaction. In fact, one of the orange regions appears near the isotropic spin condition,  $\lambda_1 = 0$  ( $\theta = 0$ ) and  $\lambda_2 = 0$ , and the other seems to be continuously connected with another isotropic point with the condition that  $J_1 = 0$  ( $\theta = \pi/2$ ) and  $\lambda_2 = 0$ . In the isotropic case with large enough second-neighbor interaction, the ground states are doubly degenerate dimerized states with spontaneous breaking of translational symmetry similar to the Majumdar–Ghosh state [107–109]. This degeneracy in the same subspace can be characterized as a (at least weak) trivial ZM. In fact, the origin of this trivial ZM, which is sublattice degree of freedom in a doubly extended unit cell with spontaneous breaking of translational symmetry induced by the second-neighbor interactions, is common to the weak trivial ZM in the dark-green and blue regions (see also Sec. III). Thus, considering the generality in physics, it may be appropriate that the weak ZM is regarded as not a Majorana ZM but just a trivial ZM. However, it is more intriguing that if there is at least one



TABLE I. Transformation to Majorana ZMs. The Majorana ZMs satisfy  $\{\tilde{\gamma}_j^\tau, \mathcal{F}\} = [\tilde{\gamma}_j^\tau, \mathcal{H}] = 0$  and  $\{\tilde{\gamma}_j^\tau, \tilde{\gamma}_{j'}^{\tau'}\} = \delta_{j,j'}\delta_{\tau,\tau'}$ . These are similar to the Jordan-Wigner transformation.

Pauli matrix	Majorana ZM	Trivial ZMs	Transformations
$\sigma^x$ (flip)	$\tilde{\gamma}_0^a$	$\zeta_j^a$	$\tilde{\gamma}_j^a = i\tilde{\gamma}_0^a \mathcal{F} \zeta_j^a \prod_{k>j} Z_k / \sqrt{2}$
$\sigma^z$ (parity)	$\mathcal{F}$	$Z_j$	
$\sigma^y$ (pair)	$\tilde{\gamma}_0^b = i\tilde{\gamma}_0^a \mathcal{F} \prod_j Z_j$	$\zeta_j^b = i\zeta_j^a Z_j$	$\tilde{\gamma}_j^b = -\tilde{\gamma}_0^a \mathcal{F} \zeta_j^a Z_j \prod_{k>j} Z_k / \sqrt{2}$

Thus, we can express the auxiliary field with the MPO representation as

$$\mathcal{H}_F = \mathbf{F}_1 \mathbf{F}_2 \cdots \mathbf{F}_{N-1} \mathbf{F}_N^T \quad (\text{A11})$$

with

$$\mathbf{F}_1 = \mu(-2\chi^x S_1^x, \quad -2\chi^y S_1^y, \quad -2\chi^z S_1^z, \quad 3), \quad (\text{A12})$$

$$\mathbf{F}_j = \begin{pmatrix} 2S_j^x & & & \\ & 2S_j^y & & \\ & & 2S_j^z & \\ & & & 1 \end{pmatrix}, \quad (\text{A13})$$

$$\mathbf{F}_N = (2S_N^x, \quad 2S_N^y, \quad 2S_N^z, \quad 1). \quad (\text{A14})$$

It is not necessary to obtain the MPO representation for another auxiliary field  $\mathcal{H}_L$ , because the operator is just a (superposed) direct product of MPS. For the first-excited state  $|1\rangle$ , the effect of  $\mathcal{H}_L$  reads

$$\mathcal{H}_L|1\rangle = \epsilon\langle 0|1\rangle|0\rangle. \quad (\text{A15})$$

Therefore, it is sufficient to calculate the inner product of two MPSs  $\langle 0|1\rangle$ .

Although the MPO representation with PBC is more complicated than that with OBC, it is available via correspondence between a single chain with PBC and a double chain coupled with two edges [see Fig. 1(b)]. In this mapping, the site index is alternately labeled in the first and second chains, that is, in Fig. 1(b),

$$\begin{aligned} & (\mathbf{S}_1, \mathbf{S}_2, \mathbf{S}_3, \dots, \mathbf{S}_{N/2}, \mathbf{S}_{N/2+1}, \dots, \mathbf{S}_{N-2}, \mathbf{S}_{N-1}, \mathbf{S}_N) \\ & \rightarrow (\mathbf{S}_1, \mathbf{S}_3, \mathbf{S}_5, \dots, \mathbf{S}_{N-1}, \mathbf{S}_N, \dots, \mathbf{S}_6, \mathbf{S}_4, \mathbf{S}_2). \end{aligned} \quad (\text{A16})$$

Thus, in appearance, longer-ranged interactions up to fourth-neighbor site are required. Note that in this form, the bond dimension of the MPO with PBC is approximately doubled as compared with OBC, and we also have to set the bond dimension of MPS much larger due to a large value of entanglement entropy.

#### APPENDIX B: A PAIR OF MAJORANA ZMS AND NUMBER OF THEM

In general, supposing that a certain parity operator  $\mathcal{Q}$  obeys  $[\mathcal{Q}, \mathcal{H}] = 0$ ,  $\{\mathcal{Q}, \tilde{\gamma}^a\} = 0$ , and  $\mathcal{Q}^2 = 1$  for a Majorana ZM  $\tilde{\gamma}^a$ , we can make a pair to the Majorana ZM by using unitary transformation,

$$\tilde{\gamma}^b = e^{-i(\pi/4)\mathcal{Q}} \tilde{\gamma}^a e^{i(\pi/4)\mathcal{Q}} = i\tilde{\gamma}^a \mathcal{Q}, \quad (\text{B1})$$

satisfying the Majorana condition  $\{\tilde{\gamma}^\tau, \tilde{\gamma}^{\tau'}\} = \delta_{\tau,\tau'}$  and commutation relation  $[\tilde{\gamma}^b, \mathcal{H}] = 0$ . In the Ising chain, this parity operator corresponds to  $\mathcal{Q} = -2i\gamma_N^b \gamma_1^a = -4S_N^x S_1^x \mathcal{F}$  for  $\tilde{\gamma}^a = \gamma_1^a$  and  $\tilde{\gamma}^b = \gamma_N^b$ . Simultaneously, we can obtain another pair to the Majorana ZM,  $(\tilde{\gamma}^b)^\gamma = i\tilde{\gamma}^a \mathcal{F} \neq \tilde{\gamma}^b$ , provided that  $\mathcal{Q} = \mathcal{F}$ , while this mode  $(\tilde{\gamma}^b)^\gamma$  does not anticommute with  $\tilde{\gamma}^b$ , i.e., these modes are essentially not independent. Although the definition of the paired Majorana ZM is not unique, only one independent Majorana ZM can be constructed by one Majorana ZM as its pair. Thus, the number of independent Majorana ZMs  $D_m$  is always even, and the degeneracy of eigenstates in the Hamiltonian corresponds to  $2^{D_m/2}$ .

#### APPENDIX C: TRANSFORMATION OF TRIVIAL ZMS TO MAJORANA ZMS

As mentioned in Sec. III, we can rewrite several trivial ZMs to Majorana ZMs, if there is an intrinsic Majorana ZM  $\tilde{\gamma}_0^a$  obeying  $\{\tilde{\gamma}_0^a, \mathcal{F}\} = [\tilde{\gamma}_0^a, \mathcal{H}] = [\mathcal{F}, \mathcal{H}] = 0$  and  $2(\tilde{\gamma}_0^a)^2 = 1$ . Here, we explicitly present the transformation of the trivial ZMs to Majorana ZMs. (In this section, we assume strong ZMs, though weak ZMs can also be considered with introducing a certain projection.) Firstly, we define the  $j$ th trivial ZM and its parity by  $\zeta_j^a$  and  $Z_j$  ( $j = 1, 2, \dots, D$ ) where  $D$  denotes the number of trivial ZMs, satisfying  $[\zeta_j^a, \tilde{\gamma}_0^a] = [\zeta_j^a, \mathcal{F}] = [\zeta_j^a, \zeta_j^a] = 0$  (independence of trivial ZMs) and  $\{\zeta_j^a, Z_j\} = [\zeta_j^a, \mathcal{H}] = [Z_j, \mathcal{H}] = 0$  (zero-energy excitations) with  $(\zeta_j^a)^2 = Z_j^2 = 1$  ( $Z_2$  quantities). The trivial ZM operator  $\zeta_j^a$  flips an eigenvalue of the parity operator  $Z_j$ , so that these can correspond to Pauli matrices  $\sigma_j^x$  and  $\sigma_j^z$  acting on a Hilbert space consisting of independent pseudospins. Hence, there is another Pauli matrix  $\sigma_j^y = i\sigma_j^x \sigma_j^z$ , which is regarded as a pair to the trivial ZM  $\zeta_j^b = i\zeta_j^a Z_j$  satisfying  $\{\zeta_j^b, Z_j\} = [\zeta_j^b, \mathcal{H}] = 0$  and  $\{\zeta_j^\tau, \zeta_{j'}^{\tau'}\} = 2\delta_{j,j'}\delta_{\tau,\tau'}$  (see Table I). These trivial ZMs can be transformed to Majorana ZMs with introducing a Jordan-Wigner phase  $\prod_{k<j} Z_k$  and a flip of fermionic parity  $i\tilde{\gamma}_0^a \mathcal{F}$ , i.e.,  $\tilde{\gamma}_j^\tau = i\tilde{\gamma}_0^a \mathcal{F} \zeta_j^\tau \prod_{k>j} Z_k / \sqrt{2}$  for  $\tau = a, b$  and  $j = 1, 2, \dots, D$ . In addition, we have to add a factor  $\prod_j Z_j$  into a pair to the intrinsic Majorana ZM  $\tilde{\gamma}_0^b = i\tilde{\gamma}_0^a \mathcal{F}$  to anticommute with other Majorana ZMs. Table I shows the correspondence of them, where every Majorana ZM obtained by the transformation is independent from the others, that is,  $\{\tilde{\gamma}_j^\tau, \mathcal{F}\} = [\tilde{\gamma}_j^\tau, \mathcal{H}] = 0$  and  $\{\tilde{\gamma}_j^\tau, \tilde{\gamma}_{j'}^{\tau'}\} = \delta_{j,j'}\delta_{\tau,\tau'}$ . Consequently, we can obtain  $(D+1)$  Majorana ZMs, if there is an intrinsic Majorana ZM and other trivial ZMs associated with any symmetry breaking.

- [1] F. Wilczek, Majorana returns, *Nat. Phys.* **5**, 614 (2009).
- [2] J. Alicea, New directions in the pursuit of Majorana fermions in solid state systems, *Rep. Prog. Phys.* **75**, 76501 (2012).
- [3] S. R. Elliott and M. Franz, *Colloquium: Majorana fermions in nuclear, particle, and solid-state physics*, *Rev. Mod. Phys.* **87**, 137 (2015).
- [4] N. Read and D. Green, Paired states of fermions in two dimensions with breaking of parity and time-reversal symmetries and the fractional quantum Hall effect, *Phys. Rev. B* **61**, 10267 (2000).
- [5] A. Y. Kitaev, Unpaired Majorana fermions in quantum wires, *Phys. Usp.* **44**, 131 (2001).
- [6] D. A. Ivanov, Non-Abelian Statistics of Half-Quantum Vortices in  $p$ -Wave Superconductors, *Phys. Rev. Lett.* **86**, 268 (2001).
- [7] J. D. Sau, R. M. Lutchyn, S. Tewari, and S. Das Sarma, Generic New Platform for Topological Quantum Computation Using Semiconductor Heterostructures, *Phys. Rev. Lett.* **104**, 040502 (2010).
- [8] A. Więckowski, M. Mierzejewski, and M. Kupczyński, Majorana phase gate based on the geometric phase, *Phys. Rev. B* **101**, 014504 (2020).
- [9] G. Goldstein and C. Chamon, Decay rates for topological memories encoded with Majorana fermions, *Phys. Rev. B* **84**, 205109 (2011).
- [10] M. Cheng, R. M. Lutchyn, and S. Das Sarma, Topological protection of Majorana qubits, *Phys. Rev. B* **85**, 165124 (2012).
- [11] J. C. Budich, S. Walter, and B. Trauzettel, Failure of protection of Majorana based qubits against decoherence, *Phys. Rev. B* **85**, 121405(R) (2012).
- [12] D. Rainis and D. Loss, Majorana qubit decoherence by quasi-particle poisoning, *Phys. Rev. B* **85**, 174533 (2012).
- [13] M. J. Schmidt, D. Rainis, and D. Loss, Decoherence of Majorana qubits by noisy gates, *Phys. Rev. B* **86**, 085414 (2012).
- [14] L. Mazza, M. Rizzi, M. D. Lukin, and J. I. Cirac, Robustness of quantum memories based on Majorana zero modes, *Phys. Rev. B* **88**, 205142 (2013).
- [15] V. Shivamoggi, G. Refael, and J. E. Moore, Majorana fermion chain at the quantum spin Hall edge, *Phys. Rev. B* **82**, 041405(R) (2010).
- [16] Y. Oreg, G. Refael, and F. von Oppen, Helical Liquids and Majorana Bound States in Quantum Wires, *Phys. Rev. Lett.* **105**, 177002 (2010).
- [17] R. M. Lutchyn, J. D. Sau, and S. Das Sarma, Majorana Fermions and a Topological Phase Transition in Semiconductor-Superconductor Heterostructures, *Phys. Rev. Lett.* **105**, 077001 (2010).
- [18] J. Alicea, Majorana fermions in a tunable semiconductor device, *Phys. Rev. B* **81**, 125318 (2010).
- [19] A. M. Cook, M. M. Vazifeh, and M. Franz, Stability of Majorana fermions in proximity-coupled topological insulator nanowires, *Phys. Rev. B* **86**, 155431 (2012).
- [20] M. T. Deng, C. L. Yu, G. Y. Huang, M. Larsson, P. Caroff, and H. Q. Xu, Anomalous zero-bias conductance peak in a Nb-InSb nanowire-Nb hybrid device, *Nano Lett.* **12**, 6414 (2012).
- [21] V. Mourik, K. Zuo, S. M. Frolov, S. R. Plissard, E. P. Bakkers, and L. P. Kouwenhoven, Signatures of majorana fermions in hybrid superconductor-semiconductor nanowire devices, *Science* **336**, 1003 (2012).
- [22] A. Das, Y. Ronen, Y. Most, Y. Oreg, M. Heiblum, and H. Shtrikman, Zero-bias peaks and splitting in an Al-InAs nanowire topological superconductor as a signature of Majorana fermions, *Nat. Phys.* **8**, 887 (2012).
- [23] L. P. Rokhinson, X. Liu, and J. K. Furdyna, The fractional a.c. Josephson effect in a semiconductor-superconductor nanowire as a signature of Majorana particles, *Nat. Phys.* **8**, 795 (2012).
- [24] J. D. Sau, C. H. Lin, H. Y. Hui, and S. Das Sarma, Avoidance of Majorana Resonances in Periodic Topological Superconductor-Nanowire Structures, *Phys. Rev. Lett.* **108**, 067001 (2012).
- [25] A. D. K. Finck, D. J. Van Harlingen, P. K. Mohseni, K. Jung, and X. Li, Anomalous Modulation of a Zero-Bias Peak in a Hybrid Nanowire-Superconductor Device, *Phys. Rev. Lett.* **110**, 126406 (2013).
- [26] H. O. H. Churchill, V. Fatemi, K. Grove-Rasmussen, M. T. Deng, P. Caroff, H. Q. Xu, and C. M. Marcus, Superconductor-nanowire devices from tunneling to the multichannel regime: Zero-bias oscillations and magnetoconductance crossover, *Phys. Rev. B* **87**, 241401(R) (2013).
- [27] S. Nadj-Perge, I. K. Drozdov, J. Li, H. Chen, S. Jeon, J. Seo, A. H. MacDonald, B. A. Bernevig, and A. Yazdani, Observation of Majorana fermions in ferromagnetic atomic chains on a superconductor, *Science* **346**, 602 (2014).
- [28] M. Okamoto, Y. Takane, and K. I. Imura, One-dimensional topological insulator: A model for studying finite-size effects in topological insulator thin films, *Phys. Rev. B* **89**, 125425 (2014).
- [29] A. P. Higginbotham, S. M. Albrecht, G. Kiršanskas, W. Chang, F. Kuemmeth, P. Krogstrup, T. S. Jespersen, J. Nygård, K. Flensberg, and C. M. Marcus, Parity lifetime of bound states in a proximitized semiconductor nanowire, *Nat. Phys.* **11**, 1017 (2015).
- [30] M. Malard, G. I. Japaridze, and H. Johannesson, Synthesizing Majorana zero-energy modes in a periodically gated quantum wire, *Phys. Rev. B* **94**, 115128 (2016).
- [31] M. Sato and S. Fujimoto, Majorana fermions and topology in superconductors, *J. Phys. Soc. Jpn.* **85**, 072001 (2016).
- [32] P. Mognini, E. van Nieuwenburg, and R. Chitra, Sensing Floquet-Majorana fermions via heat transfer, *Phys. Rev. B* **96**, 125144 (2017).
- [33] P. Mognini, W. Chen, and R. Chitra, Universal quantum criticality in static and Floquet-Majorana chains, *Phys. Rev. B* **98**, 125129 (2018).
- [34] B. Jäck, Y. Xie, J. Li, S. Jeon, B. A. Bernevig, and A. Yazdani, Observation of a Majorana zero mode in a topologically protected edge channel, *Science* **364**, 1255 (2019).
- [35] H. Pan and S. Das Sarma, Physical mechanisms for zero-bias conductance peaks in Majorana nanowires, *Phys. Rev. Res.* **2**, 013377 (2020).
- [36] S. M. Frolov, M. J. Manfra, and J. D. Sau, Topological superconductivity in hybrid devices, *Nat. Phys.* **16**, 718 (2020).
- [37] P. Mognini, Edge mode manipulation through commensurate multifrequency driving, *Phys. Rev. B* **102**, 235143 (2020).
- [38] O. Motrunich, K. Damle, and D. A. Huse, Griffiths effects and quantum critical points in dirty superconductors without spin-rotation invariance: One-dimensional examples, *Phys. Rev. B* **63**, 224204 (2001).
- [39] P. W. Brouwer, M. Duckheim, A. Romito, and F. von Oppen, Probability Distribution of Majorana End-State

- Energies in Disordered Wires, *Phys. Rev. Lett.* **107**, 196804 (2011).
- [40] P. W. Brouwer, M. Duckheim, A. Romito, and F. von Oppen, Topological superconducting phases in disordered quantum wires with strong spin-orbit coupling, *Phys. Rev. B* **84**, 144526 (2011).
- [41] A. R. Akhmerov, J. P. Dahlhaus, F. Hassler, M. Wimmer, and C. W. J. Beenakker, Quantized Conductance at the Majorana Phase Transition in a Disordered Superconducting Wire, *Phys. Rev. Lett.* **106**, 057001 (2011).
- [42] L. J. Lang and S. Chen, Majorana fermions in density-modulated  $p$ -wave superconducting wires, *Phys. Rev. B* **86**, 205135 (2012).
- [43] M. Tezuka and N. Kawakami, Reentrant topological transitions in a quantum wire/superconductor system with quasiperiodic lattice modulation, *Phys. Rev. B* **85**, 140508(R) (2012).
- [44] A. M. Lobos, R. M. Lutchyn, and S. Das Sarma, Interplay of Disorder and Interaction in Majorana Quantum Wires, *Phys. Rev. Lett.* **109**, 146403 (2012).
- [45] Y. Niu, S. B. Chung, C. H. Hsu, I. Mandal, S. Raghu, and S. Chakravarty, Majorana zero modes in a quantum Ising chain with longer-ranged interactions, *Phys. Rev. B* **85**, 035110 (2012).
- [46] W. DeGottardi, D. Sen, and S. Vishveshwara, Majorana Fermions in Superconducting 1D Systems Having Periodic, Quasiperiodic, and Disordered Potentials, *Phys. Rev. Lett.* **110**, 146404 (2013).
- [47] R. Wakatsuki, M. Ezawa, Y. Tanaka, and N. Nagaosa, Fermion fractionalization to Majorana fermions in a dimerized Kitaev superconductor, *Phys. Rev. B* **90**, 014505 (2014).
- [48] I. Adagideli, M. Wimmer, and A. Teker, Effects of electron scattering on the topological properties of nanowires: Majorana fermions from disorder and superlattices, *Phys. Rev. B* **89**, 144506 (2014).
- [49] S. S. Hegde and S. Vishveshwara, Majorana wave-function oscillations, fermion parity switches, and disorder in Kitaev chains, *Phys. Rev. B* **94**, 115166 (2016).
- [50] N. M. Gergs, L. Fritz, and D. Schuricht, Topological order in the Kitaev/Majorana chain in the presence of disorder and interactions, *Phys. Rev. B* **93**, 075129 (2016).
- [51] X. Zhu and M. Franz, Tricritical Ising phase transition in a two-ladder Majorana fermion lattice, *Phys. Rev. B* **93**, 195118 (2016).
- [52] L. Herviou, C. Mora, and K. Le Hur, Phase diagram and entanglement of two interacting topological Kitaev chains, *Phys. Rev. B* **93**, 165142 (2016).
- [53] Y. Wang, J. J. Miao, H. K. Jin, and S. Chen, Exact solution to an interacting dimerized Kitaev model at symmetric point, *Phys. Rev. B* **96**, 205428 (2017).
- [54] R. Ghadimi, T. Sugimoto, and T. Tohyama, Majorana zero-energy mode and fractal structure in Fibonacci-Kitaev chain, *J. Phys. Soc. Jpn.* **86**, 114707 (2017).
- [55] M. Pérez and G. Martínez, Polynomial description of inhomogeneous topological superconducting wires, *J. Phys.: Condens. Matter* **29**, 475503 (2017).
- [56] A. Nava, R. Giuliano, G. Campagnano, and D. Giuliano, Persistent current and zero-energy Majorana modes in a  $p$ -wave disordered superconducting ring, *Phys. Rev. B* **95**, 155449 (2017).
- [57] M. McGinley, J. Knolle, and A. Nunnenkamp, Robustness of Majorana edge modes and topological order: Exact results for the symmetric interacting Kitaev chain with disorder, *Phys. Rev. B* **96**, 241113(R) (2017).
- [58] H. Shapourian, K. Shiozaki, and S. Ryu, Many-Body Topological Invariants for Fermionic Symmetry-Protected Topological Phases, *Phys. Rev. Lett.* **118**, 216402 (2017).
- [59] J. J. Miao, H. K. Jin, F. C. Zhang, and Y. Zhou, Exact Solution for the Interacting Kitaev Chain at the Symmetric Point, *Phys. Rev. Lett.* **118**, 267701 (2017).
- [60] M. Ezawa, Exact solutions and topological phase diagram in interacting dimerized Kitaev topological superconductors, *Phys. Rev. B* **96**, 121105(R) (2017).
- [61] D. Dey, S. K. Saha, P. S. Deo, M. Kumar, and S. Sarkar, A study of topological quantum phase transition and Majorana localization length for the interacting helical liquid system, *J. Phys. Soc. Jpn.* **86**, 074002 (2017).
- [62] H. H. Hung, J. Wu, K. Sun, and C. K. Chiu, Engineering of many-body Majorana states in a topological insulator/s-wave superconductor heterostructure, *Sci. Rep.* **7**, 3499 (2017).
- [63] Y. Wang, Detecting topological phases via survival probabilities of edge Majorana fermions, *Phys. Rev. E* **98**, 042128 (2018).
- [64] S. Lieu, D. K. K. Lee, and J. Knolle, Disorder protected and induced local zero-modes in longer-range Kitaev chains, *Phys. Rev. B* **98**, 134507 (2018).
- [65] M. Thakurathi, P. Simon, I. Mandal, J. Klinovaja, and D. Loss, Majorana Kramers pairs in Rashba double nanowires with interactions and disorder, *Phys. Rev. B* **97**, 045415 (2018).
- [66] C. Monthus, Topological phase transitions in random Kitaev  $\alpha$ -chains, *J. Phys. A: Math. Theor.* **51**, 465301 (2018).
- [67] A. Więckowski, M. M. Maška, and M. Mierzejewski, Identification of Majorana Modes in Interacting Systems by Local Integrals of Motion, *Phys. Rev. Lett.* **120**, 040504 (2018).
- [68] Z. Li and Q. Han, Effect of interaction on the Majorana zero modes in the Kitaev chain at half filling, *Chin. Phys. Lett.* **35**, 47101 (2018).
- [69] J. Wouters, H. Katsura, and D. Schuricht, Exact ground states for interacting Kitaev chains, *Phys. Rev. B* **98**, 155119 (2018).
- [70] G. Kells, N. Moran, and D. Meidan, Localization enhanced and degraded topological order in interacting  $p$ -wave wires, *Phys. Rev. B* **97**, 085425 (2018).
- [71] J. J. Miao, H. K. Jin, F. C. Zhang, and Y. Zhou, Majorana zero modes and long range edge correlation in interacting Kitaev chains: Analytic solutions and density-matrix-renormalization-group study, *Sci. Rep.* **8**, 488 (2018).
- [72] A. Habibi, R. Ghadimi, S. A. Jafari, and S. Rouhani, Topological phase diagram of the disordered 2XY model in presence of generalized Dzyaloshinskii-Moriya Interaction, *J. Phys.: Condens. Matter* **32**, 015604 (2020).
- [73] L. Levy and M. Goldstein, Entanglement and disorder-enhanced topological phase in the Kitaev chain, *Universe* **5**, 33 (2019).
- [74] C. B. Hua, R. Chen, D. H. Xu, and B. Zhou, Disorder-induced Majorana zero modes in a dimerized Kitaev superconductor chain, *Phys. Rev. B* **100**, 205302 (2019).
- [75] A. Więckowski and A. Ptok, Influence of long-range interaction on Majorana zero modes, *Phys. Rev. B* **100**, 144510 (2019).

- [76] M. A. R. Griffith, E. Mamani, L. Nunes, and H. Caldas, Effects of anisotropic correlations in fermionic zero-energy bound states of topological phases, *Phys. Rev. B* **101**, 184514 (2020).
- [77] A. Kobińska, N. Sedlmayr, M. M. Maška, and T. Domański, Dimerization-induced topological superconductivity in a Rashba nanowire, *Phys. Rev. B* **101**, 085402 (2020).
- [78] I. Mahyaeh and E. Ardonne, Study of the phase diagram of the Kitaev-Hubbard chain, *Phys. Rev. B* **101**, 085125 (2020).
- [79] S. V. Aksenov, A. O. Zlotnikov, and M. S. Shustin, Strong Coulomb interactions in the problem of Majorana modes in a wire of the nontrivial topological class BDI, *Phys. Rev. B* **101**, 125431 (2020).
- [80] R. B. Wang, A. Furusaki, and O. A. Starykh, Majorana end states in an interacting quantum wire, *Phys. Rev. B* **102**, 165147 (2020).
- [81] X. L. Yu, L. Jiang, Y. M. Quan, T. Wu, Y. Chen, L. J. Zou, and J. Wu, Topological phase transitions, Majorana modes, and quantum simulation of the Su-Schrieffer-Heeger model with nearest-neighbor interactions, *Phys. Rev. B* **101**, 045422 (2020).
- [82] P. Fendley, Strong zero modes and eigenstate phase transitions in the XYZ/interacting Majorana chain, *J. Phys. A: Math. Theor.* **49**, 30LT01 (2016).
- [83] T. Sugimoto, M. Ohtsu, and T. Tohyama, Reentrant topological phase transition in a bridging model between Kitaev and Haldane chains, *Phys. Rev. B* **96**, 245118 (2017).
- [84] G. Y. Chitov, Local and nonlocal order parameters in the Kitaev chain, *Phys. Rev. B* **97**, 085131 (2018).
- [85] Z.-Y. Zheng, H.-C. Kou, and P. Li, Quaternary Jordan-Wigner mapping and topological extended-kink phase in the interacting Kitaev ring, *Phys. Rev. B* **100**, 235127 (2019).
- [86] S. K. Saha, D. Dey, M. S. Roy, S. Sarkar, and M. Kumar, Characterization of Majorana-Ising phase transition in a helical liquid system, *J. Magn. Magn. Mater.* **475**, 257 (2019).
- [87] G. Y. Chitov, T. Pandey, and P. N. Timonin, String and conventional order parameters in the solvable modulated quantum chain, *Phys. Rev. B* **100**, 104428 (2019).
- [88] G. Magnifico, D. Vodola, E. Ercolessi, S. P. Kumar, M. Müller, and A. Bermudez, Symmetry-protected topological phases in lattice gauge theories: Topological QED2, *Phys. Rev. D* **99**, 014503 (2019).
- [89] T. Pandey and G. Y. Chitov, Phase diagram and topological order in the modulated XYZ chain with magnetic field, *Phys. Rev. B* **102**, 054436 (2020).
- [90] S. Sarkar, A study of interaction effects and quantum Berezinskii-Kosterlitz-Thouless transition in the Kitaev chain, *Sci. Rep.* **10**, 2299 (2020).
- [91] D. J. Yates, A. G. Abanov, and A. Mitra, Dynamics of almost strong edge modes in spin chains away from integrability, *Phys. Rev. B* **102**, 195419 (2020).
- [92] D. J. Yates, A. G. Abanov, and A. Mitra, Lifetime of Almost Strong Edge-Mode Operators in One-Dimensional, Interacting, Symmetry Protected Topological Phases, *Phys. Rev. Lett.* **124**, 206803 (2020).
- [93] G. Magnifico, D. Vodola, E. Ercolessi, S. P. Kumar, M. Müller, and A. Bermudez, ZN gauge theories coupled to topological fermions: QED2 with a quantum mechanical  $\theta$  angle, *Phys. Rev. B* **100**, 115152 (2019).
- [94] R. R. Kumar, Y. R. Kartik, S. Rahul, and S. Sarkar, Multicritical topological transition at quantum criticality, *Sci. Rep.* **11**, 1004 (2021).
- [95] P. Jordan and E. Wigner, Über das Paulische Äquivalenzverbot, *Z. Phys.* **47**, 631 (1928).
- [96] S. A. Jafari and F. Shahbazi, Exactly solvable spin chain models corresponding to BDI class of topological superconductors, *Sci. Rep.* **6**, 32720 (2016).
- [97] A. Habibi, S. A. Jafari, and S. Rouhani, Resilience of Majorana fermions in the face of disorder, *Phys. Rev. B* **98**, 035142 (2018).
- [98] M. A. Ruderman and C. Kittel, Indirect exchange coupling of nuclear magnetic moments by conduction electrons, *Phys. Rev.* **96**, 99 (1954).
- [99] T. Kasuya, A theory of metallic ferro- and antiferromagnetism on Zener's model, *Prog. Theor. Phys.* **16**, 45 (1956).
- [100] K. Yosida, Magnetic Properties of Cu-Mn Alloys, *Phys. Rev.* **106**, 893 (1957).
- [101] P. Fendley, Parafermionic edge zero modes in Zn-invariant spin chains, *J. Stat. Mech.* (2012) P11020.
- [102] A. S. Jermyn, R. S. K. Mong, J. Alicea, and P. Fendley, Stability of zero modes in parafermion chains, *Phys. Rev. B* **90**, 165106 (2014).
- [103] J. Alicea and P. Fendley, Topological Phases with Parafermions: Theory and Blueprints, *Annu. Rev. Condens. Matter Phys.* **7**, 119 (2016).
- [104] U. Schollwöck, The density-matrix renormalization group in the age of matrix product states, *Ann. Phys. (NY)* **326**, 96 (2011).
- [105] S. R. White, Density Matrix Formulation for Quantum Renormalization Groups, *Phys. Rev. Lett.* **69**, 2863 (1992).
- [106] S. R. White, Density-matrix algorithms for quantum renormalization groups, *Phys. Rev. B* **48**, 10345 (1993).
- [107] C. K. Majumdar and D. K. Ghosh, On next-nearest-neighbor interaction in computational studies of quantum spin systems I, *J. Math. Phys.* **10**, 1388 (1969).
- [108] C. K. Majumdar, Antiferromagnetic model with known ground state, *J. Phys. C: Solid State Phys.* **3**, 911 (1970).
- [109] T. Hikihara, M. Kaburagi, and H. Kawamura, Ground-state phase diagrams of frustrated spin-SXXZ chains: Chiral ordered phases, *Phys. Rev. B* **63**, 174430 (2001).
- [110] A. P. Schnyder, S. Ryu, A. Furusaki, and A. W. W. Ludwig, Classification of topological insulators and superconductors in three spatial dimensions, *Phys. Rev. B* **78**, 195125 (2008).
- [111] In general, the Hilbert subspace in the anisotropic XYZ spin chain can be classified with only the fermionic parity  $\mathcal{F} = \mathcal{F}^z$  and the spin-flip operator  $\mathcal{F}^x$ , i.e.,  $\mathcal{F}^y$  is not necessary. In this paper, however, we use a more symmetric form by introducing  $\mathcal{F}^y$ . This representation is useful when we consider a corresponding model via an SU(2) rotation.